Thermal-spike theory of sputtering: The influence of elastic waves in a one-dimensional cylindrical spike

Mario M. Jakas*
Departamento de Fisica Fundamental y Experimental, Universidad de La Laguna, 38201 La Laguna, Tenerife, Spain and Department of Engineering Physics, University of Virginia, Charlottesville, Virginia 22903

Eduardo M. Bringa
Department of Engineering Physics, University of Virginia, Charlottesville, Virginia 22903
(Received 7 December 1999)

The sputtering yield (Y) from a thermal spike is calculated using an extended version of the standard thermal-spike theory, which includes the transport of mass, a more realistic heat capacity, and melting. The results show that introducing the heat of melting and using a heat capacity that accounts for the ''equipartion theorem'' at low temperatures has a significant influence on the sputtering yield at low deposited energies (dE/dX). The transport of mass within the spike becomes relevant at large deposited energies, where the thermal pressure in the hot core of the spike gives rise to an elastic wave which expands and cools the spike, lowering the sputtering yield.

I. INTRODUCTION

Bombardment of a solid by energetic particles may result in the ejection of atoms from the surface. This phenomenon, known as *sputtering*, is a consequence of the collision cascade produced by the incoming projectile and higher generation of recoil atoms within the target. Moving atoms in the cascade may eventually reach the surface and, provided that the kinetic energy is large enough to overcome the attractive potential of the solid, they may escape from the solid and become sputtered. Depending on whether the density of moving atoms is either low or high, two distinct scenarios occur. When the density of moving atoms is small so that the probability of collision between two moving atoms is negligible, the sputtering is said to be *linear*. A consequence of such a linearity is that the sputtering yield (Y), i.e., the number of ejecta per incoming particle, is a linear function of the energy deposited at the surface (dE/dX). This is defined as the mean kinetic energy left by the incoming particle per unit thickness at the surface. This linear regime is fairly well understood, as evidenced by the good agreement found between theoretical models and a considerable amount of experimental data.[1,2]

When the probability of collisions between moving atoms is non-negligible the sputtering process becomes *nonlinear* and several problems arise. As one enters the realm of nonlinear energy transport processes, the mechanisms leading to sputtering become less obvious and, consequently, less amenable to theoretical treatment. In spite of that, several nonlinear models have been proposed.[3] Among them, and perhaps due to its conceptual simplicity as well as its mathematical tractability, the thermal-spike theory is the approach most often used in this regime.[4–6] The spike theory assumes that the moving atoms in the target achieve, quickly, a state of local thermal equilibrium. Therefore, if the density is assumed to remain constant, the local temperature suffices to determine the thermodynamical state of the system. The deposited energy then relaxes according to the heat conduction equation and the sputtering can be readily obtained as the flux of atoms evaporated from the hot surface. One testable outcome of this theory is that, under quite general conditions, the sputtering yield for a cylindrical excitation geometry is a quadratic function of the deposited energy, $Y \propto (dE/dX)^2$ at large dE/dX.[7,8] Such a quadratic behavior of Y was in fact observed in many experiments, and it appeared to be so firmly established that a larger-than-linear sputtering yield often is sufficient to conclude that a thermal spike occurred.

Recent molecular dynamics (MD) studies[9,10] (see Fig. 3, below) suggest that even under conditions for which spike theories predict a quadratic dependence, the sputtering yield is much closer to a linear function of dE/dX. These striking results were quite unexpected. Since the MD simulations in those papers give the most complete realization of a thermal spike one can have, the question arises: What is wrong with the standard thermal-spike theory (STST) of sputtering?

Looking at the results of MD simulations, one can see the target being disrupted during energy relaxation (see Fig. 1). Actually, most atoms within the core of the spike are seen to move away from it, leaving a ''hole'' behind and compressing the surrounding material to fairly high densities. In order to assess the importance that these expansions and compressions of the target may have for the sputtering process, a thermal spike that includes the transport of mass is evaluated here. To this end, the classical hydrodynamics equations are solved. Therefore, apart from temperature, two more variables must be added to the problem—namely, the density and the velocity of the fluid.

To directly compare standard thermal-spike models, a cylindrical spike taking place within an infinite target is evaluated, for which the hydrodynamics equations—instead of the heat conduction alone—are used to obtain the temperature profile along the radial direction. Finally, as in the STST, the sputtering yield is obtained as the evaporation of atoms from an ideal plane representing the surface. A similar study was recently performed by Martynenko and Umansky.[11] In that

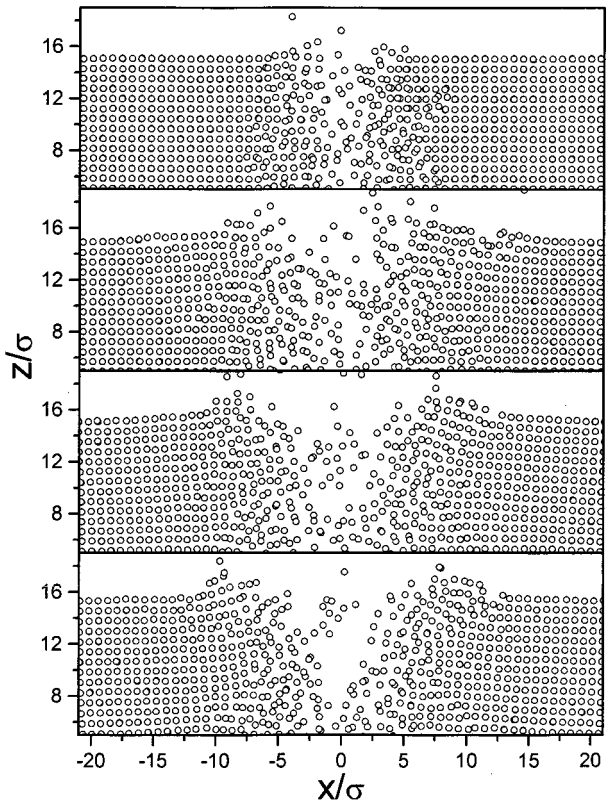

FIG. 1. Snapshots of a molecular dynamics calculation for a frozen Ar target after depositing 5.85 eV/Å within a cylindrical region of radius 2σ. From top to bottom: 0.59, 2.72, 5.39, and 7.23 ps after excitation. Only a small fraction of the sample is shown.

paper the effects of elastic waves on a thermal spike were investigated. It was shown that the amount of energy available for atomic displacements could be as low as 50% of that initially deposited by the ion. However, the consequences of this upon the sputtering yield were left unexplored. Calculations of the sputtering yield from temporarily compressed materials were published, but the approximations used were crude. Unless a more rigorous theoretical analysis confirms their range of validity, one cannot rely on such predictions.[12–14]

Comparisons of the present results with experiments are purposely omitted here. Instead, previous MD results in Ref. 10 will be used as the correct outcome of a full calculation. Such a comparison is valid as, in the MD simulations of the energy transport, the participating mechanisms are all known. This is not generally the case for a real target, thus making a comparison between present theory and experiments much more complicated and less clear. Nevertheless, MD simulations differ from calculations in this paper in several aspects. For example, MD uses a crystalline target whereas, here, one deals with an isotropic, continuous medium. Similarly, MD assumes an initial ''δ'' energy distribution in contrast with the Maxwellian used in present calculations. In spite of this, the comparison with previous MD simulations appears adequate for including the transport of mass in a sputtering calculation. Although calculations in this paper can be readily extended to other systems, all those parameters whose values are not explicitly indicated correspond to that of a solid argon. However, the sputtering yield for these cases seems to scale with the binding energy and material density for a wide range of materials.[15]

TABLE I. Unless explicitly indicated, the values listed were used in the present calculations.

Property	Symbol	Value
Atomic number density	N_0	0.026 atom/Å^3
Speed of sound	c_0	17 Å/ps
Melting temperature	$T_{\rm fus}$	200 K
Heat of melting	$Q_{\rm fus}$	0.012 eV/atom

This paper is organized as follows: in Sec. I the basics equations and assumptions used with these calculations are described. Results and discussions are contained in Sec. II. Finally, conclusions and remarks are given in Sec. III.

II. THEORETICAL ASPECTS

In the same manner as in the standard thermal-spike theory (see Ref. 6), it is assumed here that the specific energy loss of the projectile, dE/dX, translates both quickly and totally into the kinetic energy of the atoms contained within a cylindrical region of radius $r_{\rm cyl}$. Hence the mean kinetic energy $E_{\rm exc}$ per atom becomes

$$E_{\rm exc}=(dE/dx)/(\pi r_{\rm cyl}^2 N_0),$$

where N_0 is the atomic number density of the target at room temperature (see Table I) and pressure, and the initial temperature of the cylinder, $T_{\rm exc}$, is defined as

$$E_{\rm exc}=\int_0^{T_{\rm exc}} C_V(T)\,dT, \tag{1}$$

where C_V is the heat capacity per atom at constant volume.

At this point this analysis departs from the standard model and assumes that the target constitutes a classical, compressible fluid that is completely characterized by its temperature T, atomic number density N and velocity v. Therefore, assuming that the cylindrical spike takes place within an infinite solid, T, N and v depend only on the radial coordinate and change with time according to the hydrodynamics equations[16]

$$\frac{\partial N}{\partial t}=-\frac{\partial(rvN)}{r\partial r}, \tag{2}$$

$$\frac{\partial v}{\partial t}=-v\frac{\partial v}{\partial r}-\frac{1}{NM}\frac{\partial P}{\partial r}+\delta_r v_{\rm vis}, \tag{3}$$

$$\frac{\partial T}{\partial t}=-v\frac{\partial}{\partial r}T+(NC_V)^{-1}\left[\frac{\partial}{r\partial r}\left(rK_T\frac{\partial T}{\partial t}\right)-T\left(\frac{\partial P}{\partial T}\right)_N\frac{\partial(rv)}{r\partial r}+\delta_r Q_{\rm vis}\right], \tag{4}$$

where M is the atomic mass of the target, P is the pressure, and K_T is the thermal conductivity. Similarly, $\delta_r v_{\rm vis}$ and $\delta_r Q_{\rm vis}$ stand for the rate of velocity and heat change due to viscosity, respectively.

Viscosity terms were added for numerical rather than physical reasons. In fact, at the time of solving the hydrodynamics equations, numerical integration schemes are normally *unstable* and tend to amplify high-frequency spatial oscillations to the point of becoming useless after a few time steps. Since viscosity does exactly the opposite, it brings stability to the numerical scheme and makes it more robust in the sense that both larger spatial grids and time steps can be used for same accuracy. For such reasons the following formulas are introduced:

$$\delta_r v_{\rm vis} = \frac{\eta}{M_2 N}\left[\frac{\partial^2 v}{\partial r^2} + \left(\frac{\partial v}{\partial r}\right)^2 - \frac{v}{r^2}\right] \tag{5}$$

and

$$\delta_r Q_{\rm vis} = \eta\left[\left(\frac{\partial v}{\partial r}\right)^2 + \left(\frac{\partial v}{\partial r}\right)^2\right], \tag{6}$$

where η is the so-called dynamics viscosity coefficient.

In STST the heat capacity is assumed to be a power of T, i.e., $C_V = C_0 T^m$,[17,7] where m is often set to 0 and $C_0 = (3/2)k_B$, so that C_V becomes identical to that of an ideal gas, i.e., $C_V^{(\rm ideal)} = (3/2)k_B$, where k_B is Boltzmann's coefficient. In a real solid, however, the equipartition of energy states that for temperatures not much greater than that of melting (T_f) one should have $C_V \approx 2C_V^{(\rm ideal)}$. Therefore, here it is assumed that

$$C_V(T) = \begin{cases} 3k_B & T \leqslant T_f, \\ (3/2)k_B & T > T_f. \end{cases} \tag{7}$$

In addition, the heat of melting is introduced by adding the heat of fusion when T passes through the temperature of fusion T_f, that is,

$$C_V(T) \rightarrow C_V + Q_{\rm fus}/10 \quad \text{if } |T - T_f| \leqslant 5 \text{ K},$$

where $Q_{\rm fus}$ is the heat of fusion *per atom*.

The heat conduction coefficient is replaced by that in Ref. 18:

$$K_T = \frac{25}{32}\frac{k_B}{\sigma_0}\sqrt{\frac{k_B T}{\pi M_2}}, \tag{8}$$

where $\sigma_0 = 1.151\ \text{Å}^2$ is the scattering cross section. Although using Eq. (8) may not be entirely correct at solid density, it suffices for present calculations since, as is shown in Ref. 8, *the quadratic dependence of the sputtering yield did not appear to be sensitive to the approximation used for* K_T.

The pressure is assumed to be a function of both temperature and density. Here the approximation used in Ref. 19 is adopted, according to which P is split into two terms

$$P = P_T + P_C, \tag{9}$$

where P_T is the so-called thermal pressure and P_C is the crystal pressure. The former can be written as[20]

$$P_T = \lambda N k_B T, \tag{10}$$

λ being a numerical constant. And P_C can be approximated as[19]

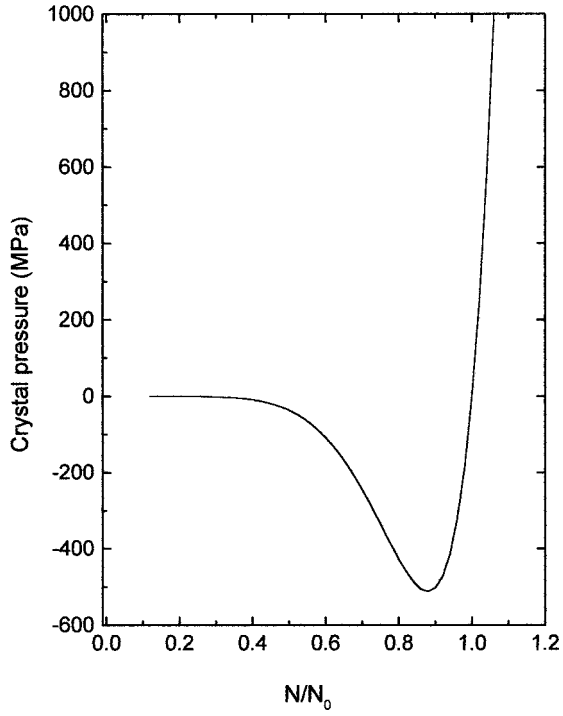

FIG. 2. Crystal pressure as a function of relative number density N/N_0: cf. Eq. (11).

$$P_C = (N_0 M_2 c_0^2/\mu)(N/N_0)^\nu[(N/N_0)^\mu - 1], \tag{11}$$

where c_0 is the speed of sound at $T = 0$ K, and μ and ν are two numerical constants. These are not independent, since the following equation must hold:

$$U_{\rm pot}(N) = \frac{1}{N_0}\int_0^{N/N_0} dx\,\frac{P_C(x)}{x^2}, \tag{12}$$

where $U_{\rm pot}$ is the mean potential energy per atom [$U_{\rm pot}(N_0) = U_0$, U_0 being the binding energy at normal density]. Moreover, $\nu > 1$; otherwise, the integral in Eq. (12) diverges. In this paper $\mu = 2$ and so $\nu = \sqrt{1 + M_2 c_0^2/U_0}$. Slight variations in the value of μ did not change the results significantly.

Figure 2 illustrates the crystal pressure in Eq. (11) as a function of N/N_0. Note that P_C becomes exceedingly large for densities larger than normal and turns negative for $N < N_0$, whereas P_C approaches zero continuously as $N \rightarrow 0$. This negative pressure accounts for the attractive force between the atoms that keeps matter at normal density.

Since P_T is responsible for coupling temperature with pressure, by setting $\lambda = 0$ the whole problem reduces to the STST. This fact will be used as a mean of going from the more complete hydrodynamics model back to the STST. It must be clearly stated, however, that the expressions above constitute convenient approximations to the pressure function in Eqs. (3) and (4) and that no accuracy regarding them and the Lennard-Jones target in the MD simulations is claimed.

By introducing these expressions into the hydrodynamics equations, the initial value problem for a cylindrical spike with an initial temperature $T_{\rm exc}$ can be solved, i.e.,

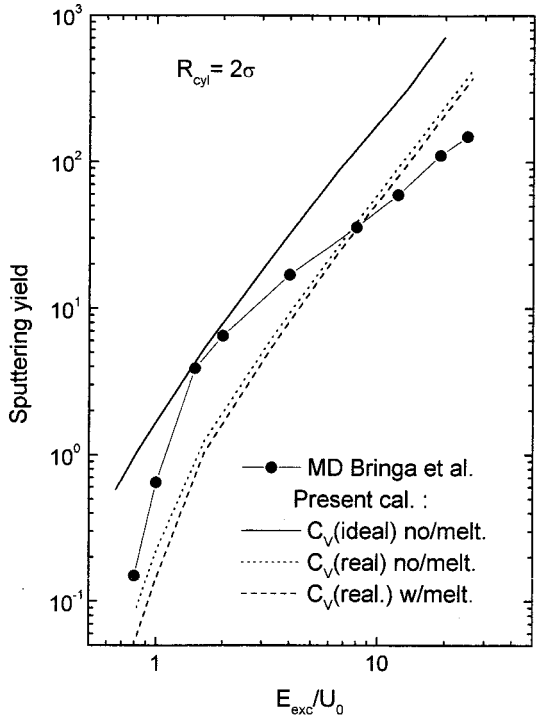

FIG. 3. Sputtering yield as a function of deposited energy. Solid symbols: molecular dynamics simulations for a sample with free surface (Ref. 10) and for a sample with PBCZ (Ref. 24). Present calculations appear as lines. In the three cases $\lambda=0$ and $C_V=C_V^{(\mathrm{ideal})}$ and no melting (solid line), $C_V=C_V^{(\mathrm{real})}$ and no melting (dashed line), and $C_V=C_V^{(\mathrm{real})}$ with melting (dot-dashed line).

$$T(0,r)=\begin{cases} T_{\mathrm{exc}} & r\leqslant r_{\mathrm{cyl}} \\ 0 & \text{otherwise} \end{cases} \tag{13}$$

together with $\nu(0,r)=0$ and $N(0,r)=N_0$.

Finally, once $T(t,r)$ is obtained, the sputtering yield is calculated as

$$Y=2\pi\int_0^\infty dt\int_0^\infty r\,dr\,\Phi(t,r), \tag{14}$$

with the flux[6,21]

$$\Phi(t,r)=N\sqrt{k_BT/2\pi M}\,\exp(-U_s/k_BT), \tag{15}$$

where $U_s=\frac{2}{3}U_{\mathrm{pot}}(N)$ is the binding energy of an atom in the surface.[10]

III. RESULTS AND DISCUSSION

To assess the importance of melting and the more realistic heat capacity in Eq. (7), the sputtering yield is first calculated assuming there is no melting and equating C_V to that of an ideal gas, i.e., $C_V=C_V^{(\mathrm{ideal})}=\frac{3}{2}k_B$. Second, C_V is replaced by that in Eq. (7) with and without melting, respectively. In all these cases, however, λ was set to 0, so that mass transport is suppressed. The results are plotted in Fig. 3 where it can be readily seen that the sputtering yields obtained using Eq. (7) are smaller than those obtained by ignoring melting and using the heat capacity of an ideal gas. Furthermore, the difference increases as the deposited energy gets smaller. This is somewhat obvious since C_V in Eq. (7) will necessarily lead to smaller T_{exc} compared to that one would obtain using $C_V^{(\mathrm{ideal})}$; cf. Eq. (1). Although discrepancies are still present in an absolute sense, the use of Eq. (7) leads to a better agreement between the shape of the $Y(dE/dX)$ calculated here and that of MD calculations at low deposited energies. At large dE/dX, however, the present results overestimate the MD yields and, more importantly, they still exhibit a nearly quadratic dependence.

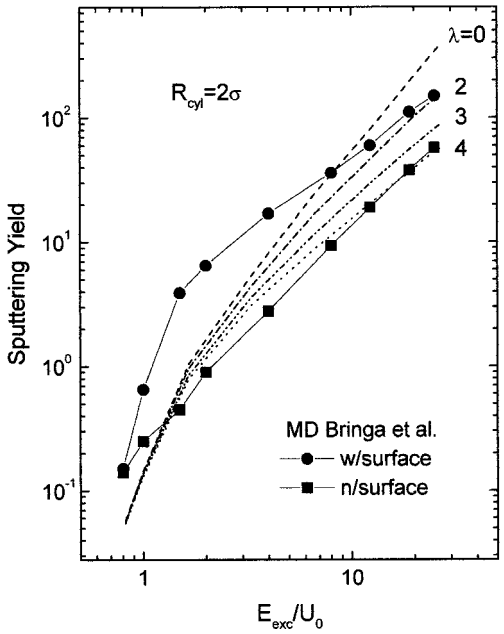

FIG. 4. Sputtering yield as a function of deposited energy for $C_V=C_V^{(\mathrm{real})}$ and several values of the thermal pressure coefficient λ [cf. Eq. (10)]. Solid squares: sputtering yields using Eqs. (14) and (15) and the temperature profile obtained from MD results for a target with periodic boundary conditions along the spike axis.

As soon as one makes $\lambda>0$, the whole process looks different and the yield also deviates from that of STST. This can be seen in Fig. 4 where the sputtering yields obtained using the hydrodynamics equations (2), (3), and (4) are plotted. Although the sputtering yields so obtained appear to be smaller than those obtained using MD, it increases with deposited energy in a manner more similar to the simulations. That is, as E_{exc}/U_0 becomes larger than approximately 1.5, Y bends over, thus becoming a less-than-quadratic function of dE/dX. This signifies that the transport of mass is in fact taking energy away from the spike, thus reducing the sputtering yield.

A better comparison between calculations in this paper and MD, however, would require MD to have a infinite target as well. To this end the MD code was run using periodic boundary conditions along the spike axis (PBCZ). For PBCZ there is no surface, so there is no ejection as well. Therefore, the sputtering yields are obtained following the same approach as in the hydrodynamics calculations here. That is, the temperature profiles obtained with MD using PBCZ are replaced in Eqs. (14) and (15), and thus the sputtering yields for an ''infinite'' target are obtained. These results[24] appear in Fig. 4 as solid squares and are labeled as ''no-surface.'' As one can readily see, MD with PBCZ and the present results, particularly those for $\lambda=4$, compare remarkably

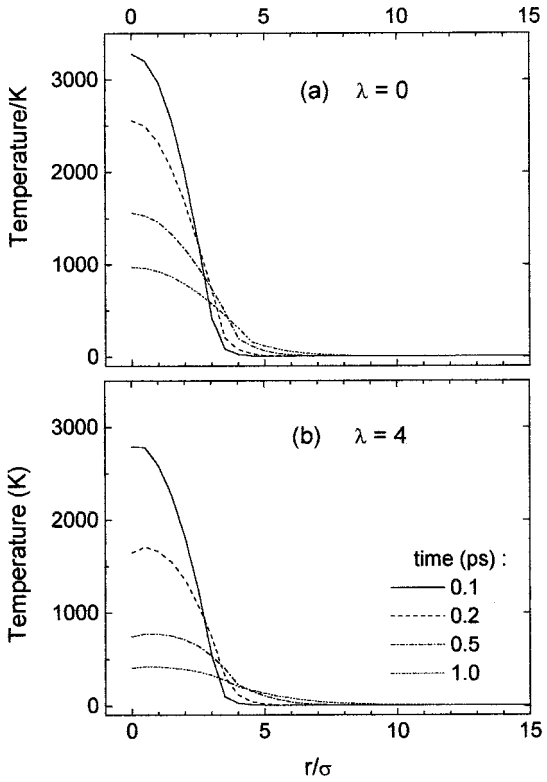

FIG. 5. Profile of temperature within the spike at different times according to STST (a) and using the hydrodynamics equations (b).

well. This indicates that the energy transport processes are well described by the model calculation here. In addition, as was discussed in Ref. 24, the difference observed between the MD calculation with and without a surface stresses the importance the surface has on the transport of energy and, consequently, on the sputtering processes.

Figures 5(a) and 5(b) show the temperature profile within the spike at different times for $\lambda=0$ and 4, respectively. As one can see, the transport of mass leads to temperature profiles that drop faster compared to the case of STST. Another interesting aspect of this process is shown in Fig. 6, where the density profile is calculated for $\lambda=2$, $E_{\rm exc}/U_0=3.3$, and $t=0.5$, 1, 2, and 4 ps, respectively. There is a clear indication that a wave is propagating from the center of the spike and a net, outwardly transport of mass is produced, giving rise to a ''hole'' or an emptied region around the origin. The front of the wave moves at a velocity that is slightly greater than the speed of sound at 0 K, i.e., c_0.

The occurrence of a hole and the fast cooling of the spike are closely connected. As is known, the expansion of the hot core is accompanied by an absorption of thermal energy and energy is delivered to the cold surrounding material, mainly as mechanical energy (compression). However, once the conversion of thermal to mechanical energy takes place, an elastic wave is triggered and the energy is carried away from the spike in an efficient manner.

Another consequence of the cooling that follows the expansion of the hot core is observed in the much faster drop-down in the ejection-time distribution. This is plotted in Fig. 7 where one can readily see that with increasing λ late ejections are suppressed. This result was observed in MD simulations and, occasionally, it was a cause of concern since the

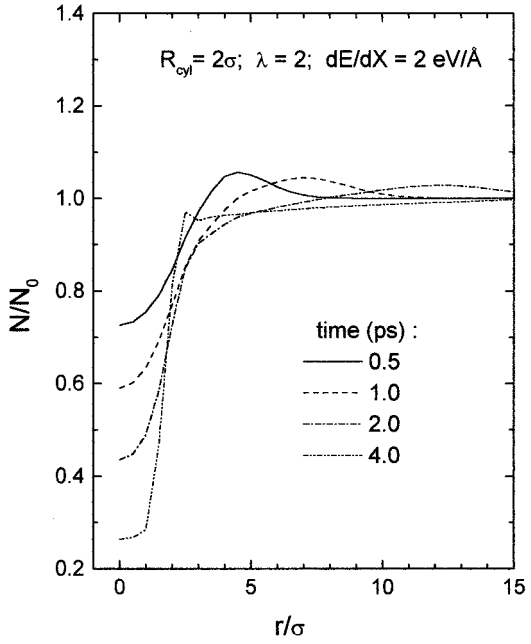

FIG. 6. Density number as a function of position and for different times during the spike.

lack of late ejections was to some extent at odd with predictions of the thermal-spike model.

The conversion of thermal to mechanical energy is best shown in Fig. 8. There, the total thermal energy (per unit depth) defined as

$$\left(\frac{dE}{dX}\right)_{\rm thermal}=2\pi\int_0^\infty dr\, rN(r,t)\int_0^{T(r,t)} dT\, C_v(T) \quad (16)$$

is plotted after division by the initial deposited energy dE/dX and for values of dE/dX ranging from 1 to 8 eV/Å and $\lambda=2$. As one can readily see, the thermal energy de-

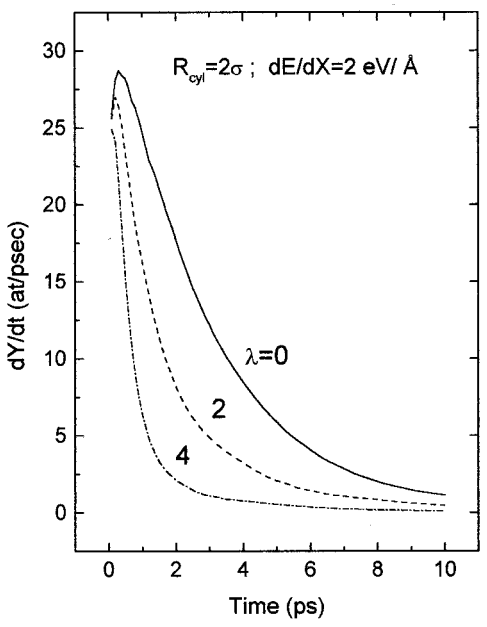

FIG. 7. Ejection time distribution.

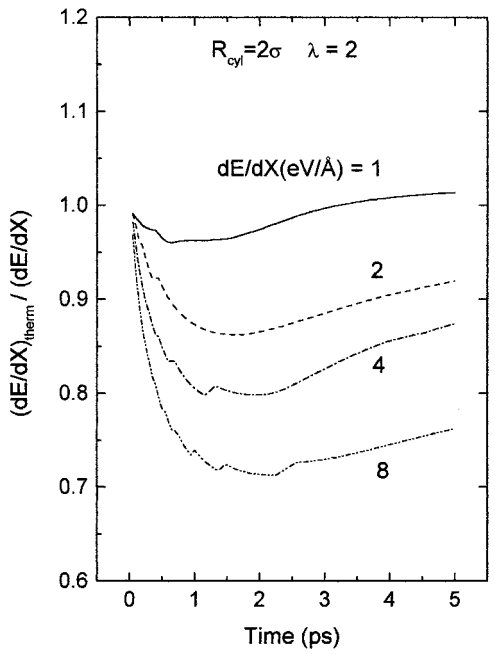

FIG. 8. Total thermal energy in the spike as a function of time: cf. Eq. (16).

creases with time very rapidly. And the fraction of the initial energy that goes into mechanical energy increases with increasing the deposited energy. At approximately 1 ps the thermal energy appears to reach its minimum and slowly recovers from then on. This is not significant for the sputtering process since, as heat has spread over a large volume, the temperature remains well below the level required to produce further ejections.

The low yield obtained in this paper, as compared to the full MD, may be attributed to the fact that the flux of sputtered particles is not well described by Eq. (15). This equation describes an undisturbed solid surface with only a small fraction of atoms having enough kinetic energy to overcome the potential barrier in the surface and escaping. In an overheated surface, where nearly all atoms are capable of escaping to vacuum, the assumptions leading to Eq. (15) do not hold.[22] In fact, according to recent calculations in a forthcoming paper[23] which include the surface, it appears that the surface performs a nearly ''explosive'' expansion and the drift velocities may reach values several times larger than that assumed in obtaining the evaporation expression in Eq. (15).

The relevance that the parameter λ has on our calculation of sputtering is obtained from Eqs. (10) and (9), and one has

$$\lambda = \frac{1}{Nk_B}\left(\frac{dP}{dT}\right)_N = \frac{\beta}{\kappa}, \tag{17}$$

where β and κ are the *thermal expansivity* and the *compressibility* of the material, respectively. According to our results, materials with a large β/κ would be less susceptible to developing a ''standard'' thermal spike and vice versa. This point was studied in a previous publication,[24] but the results were not conclusive. That is, in an attempt to change λ by modifying the interatomic potential, it was not clear whether or not other material properties in the simulation might have also been changed.

Before concluding, it is worthwhile noting that results in this paper may shed light on the point raised in Ref. 25 after the unsuccessful attempt to simulate nonlinear sputtering for heavy ions impinging on heavy targets. In fact, in the quest of simulating a thermal spike, the impact of 0.5–500 keV/amu gold clusters on a gold target were studied using a multiple-interaction computer code. These ions-target combinations are proved to give rise to high-energy density collision cascades and the occurrence of thermal spikes is justifiably expected. The results of such simulations, however, showed that the sputtering yield was a nearly linear function of the deposited energy, in a clear contradiction to the quadratic dependence predicted by STST. According to the present results, the reason for such a discrepancy may be attributed to the fact that STST ignores the elastic waves that take place during an earlier stage of the collision cascade which lowers the temperature of the spike and, consequently, reduces the amount of energy available for sputtering.

IV. CONCLUSIONS

The standard thermal-spike model has been extended to include melting, a more realistic heat capacity, and the transport of mass within the spike. To this end the fluid dynamics equations are solved for an infinite cylindrical spike of radius 2σ, σ being the Lennard-Jones length, which, in the case of Ar, is $\sigma = 3.405$ Å. It is found that (a) at low deposited energies both melting and the use of a more realistic heat capacity lead to a lower sputtering yield; (b) the transport of mass has a significant impact on the transport of energy within the spike, which becomes noticeable at large deposited energies; and (c) the transport of mass gives rise to an elastic wave that propagates at approximately the speed of sound, carrying energy away from the hot core of the spike. This ''elastic wave'' cannot be disregarded in spike calculations and, most importantly, it seems that thermal spikes may not be necessarily linked to a quadratic behavior of the sputtering yield measured in a number of experiments. Before finalizing these conclusions, this calculation will be extended to a two-dimensional spike that contains a solid/vacuum interface. In the same manner that pressure expands matter outward in the radial direction, it will also push matter along the track and into the vacuum. In that case, the expansion will interfere with the process of ejection.

ACKNOWLEDGMENTS

The authors would like to acknowledge support from the Astronomy and Chemistry Divisions of the U.S. National Science Foundation. One of us (M.M.J.) thanks the Ministry of Educación y Cultura (MEC) and the Consejería de Eduación, Cultura y Deportes del Gobierno Autónomo de Canarias (Spain) for financial support. Thanks are due to Professor R. E. Johnson for fruitful discussions and a critical reading of this manuscript.

*Corresponding author. Email address: mmateo@ull.es

[1] M. W. Thompson, Philos. Mag. **18**, 377 (1968).
[2] P. Sigmund, Phys. Rev. **184**, 383 (1969).
[3] See, for example, C. T. Reimann, Mat. Fys. Medd. K. Dan. Vidensk. Selsk. **43**, 351 (1993) and references therein.
[4] R. E. Johnson, M. Pospieszalka, and W. L. Brown, Phys. Rev. B **44**, 7263 (1991).
[5] H. H. Andersen, A. Brunelle, S. Della-Negra, J. Depauw, D. Jacquet, Y. Le Beyec, J. Chaumont, and H. Bernas, Phys. Rev. Lett. **80**, 5433 (1998).
[6] P. Sigmund and C. Claussen, J. Appl. Phys. **52**, 990 (1981).
[7] R. E. Johnson and R. Evatt, Radiat. Eff. **52**, 187 (1980).
[8] M. M. Jakas, Radiat. Eff. Defects Solids **152**, 157 (2000).
[9] H. M. Urbassek, H. Kafemann, and R. E. Johnson, Phys. Rev. B **49**, 786 (1994).
[10] E. M. Bringa and R. E. Johnson, Nucl. Instrum. Methods Phys. Res. B **152**, 167 (1999).
[11] Yu. V. Martynenko and M. V. Umansky, Radiat. Eff. Defects Solids **132**, 31 (1994).
[12] Y. Kitazoe, N. Hiraoka, and Y. Yamamura, Surf. Sci. **111**, 381 (1981).
[13] R. Kelly, Nucl. Instrum. Methods Phys. Res. B **46**, 441 (1990).
[14] H. M. Urbassek and J. Michl, Nucl. Instrum. Methods Phys. Res. B **22**, 480 (1987).
[15] E. M. Bringa, R. Johnson, and M. Jakas, Phys. Rev. B **60**, 15 107 (1999).
[16] P. Rèsibois and M. De Leener, *Classical Kinetic Theory of Fluids* (Wiley, New York, 1977).
[17] G. H. Vineyard, Radiat. Eff. **29**, 245 (1976).
[18] P. Sigmund, Appl. Phys. Lett. **25**, 169 (1974).
[19] Yu. B. Zel'dovich and Yu. P. Raizer, *Physics of Shock Waves* (Academic, New York, 1969).
[20] T. M. Reeds and K. E. Gubbins, *Applied Statistical Mechanics* (McGraw-Hill, New York, 1973).
[21] R. E. Johnson and J. Schou, Mat. Fys. Medd. K. Dan. Vidensk. Selsk. **43**, 403 (1993).
[22] F. Reif, *Fundamentals of Statistical and Thermal Physics* (McGraw-Hill, New York, 1965).
[23] M. M. Jakas (unpublished).
[24] E. M. Bringa, M. M. Jakas, and R. E. Johnson, Nucl. Instrum. Methods Phys. Res. B **164-165**, 762 (2000).
[25] M. M. Jakas and D. E. Harrison, Jr., Phys. Rev. Lett. **55**, 1782 (1985).